Texture Identification and Object Recognition Using a Soft Robotic Hand Innervated Bio-inspired Proprioception*

Yadong Yan, Chang Cheng, Mingjun Guan, Jianan Zhang, and Yu Wang*

***Abstract*—In this study, we innervated bio-inspired proprioception into a soft hand, enabling a robust perception of textures and object shapes. The tendon-driven soft finger with three joints, inspired by the human finger, was detailed. With tension sensors embedded in the tendon that simulate the Golgi tendon organ of the human body, 17 types of textures can be identified under uncertain rotation angles and actuator displacements. Four classifiers were used and the highest identification accuracy was 98.3%. A three-fingered soft hand based on the bionic finger was developed. Its basic grasp capability was tested experimentally. The soft hand can distinguish 10 types of objects that vary in shape with top grasp and side grasp, with the highest accuracies of 96.33% and 96.00%, respectively. Additionally, for six objects with close shapes, the soft hand obtained an identification accuracy of 97.69% with a scan-grasp method. This study offers a novel bionic solution for the texture identification and object recognition of soft manipulators.**

I. Introduction

Soft manipulators have been studied widely owing to their inherent compliance during interactions with objects and the environment [1-3]. Some studies have also realized delicate in-hand manipulations[4-6]. However, adequately endowing robots with a "sense of touch" remains a challenge [7, 8]. Considerable work has focused on flexible, surface-mountable tactile sensors to realize texture recognition[9, 10] and mimic the human cutaneous mechanoreceptive system to achieve tactile sensation in robotic hands [11-13]. However, these types of sensors have difficulty densely covering the entire manipulator, which means that the sensitive area is confined. Moreover, recalibration is generally required for changes in contact conditions, such as the contact angle and actuate state [14]. All of these drawbacks limit the application of these sensors.

Recent work has shown that proprioception is an effective method for enabling robotic hand sensory ability. In Zhao's work, they innervated a soft robotic hand via optical waveguides to detect the shapes and textures of objects [15]. In addition, an analogous sensor was used to measure the curvature of the soft structure in [16]. By embedding bend sensors into soft fingers, the soft hand in [17] can identify different objects that vary in shape. In Luca's work, they reconstructed the shape of a soft finger using a hexagonal tactile array placed at the base of the cylinder finger [18]. Compared to achieving tactile sensation with surface-mountable sensors, proprioceptive sensors are usually more compact in integration and robust to changes in external conditions. Given these benefits, this study developed a soft hand that mimics the human proprioception framework. As shown in Fig. 1, by the tension sensor embedded in the tendon of the finger, the dynamic changes of the tendon force can be recorded in contact, which we used to recognize textures. The bionic finger can classify 17 textures under various contact angles and actuator displacements without recalibration. Based on this, a three-fingered soft hand was developed to recognize objects.

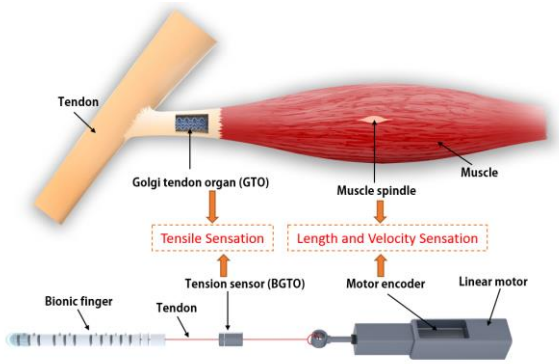

Fig. 1 The framework of the bionic design.

In general, object recognition relies on the difference in object shape, as in [17]. For objects with the same shape, this type of method is difficult to identify. Although some studies have identified the object relying on other information, for instance, in [19], the robotic hand identified the object based on the temperature, contact pressure, and thermal conductivity information. However, these methods rely on highly complex sensors and require accurate contact. In this study, we identified six cylinders with identical geometries using universal one-dimensional force sensors. This approach was robust to changes in contact conditions and was simple to integrate into other tendon-driven systems.

In this paper, Section II describes the design of the bionic finger and the three-fingered soft hand. In addition, the basic grasp ability was verified. A set of experiments was conducted in Section III, which shows the perception of textures of the bionic finger. The object recognition capacity is illustrated in Section IV. Section V presents the conclusion and discussion of this paper.

*Research supported by "National Key R&D Program of China" under Grant 2017YFA0701101.

Y. Yan, M. Guan, J. Zhang, Y. Wang are with the School of Biological Science and Medical Engineering, Beihang University, Beijing 100191, China (e-mail: adam7217@qq.com, 247864189@qq.com, baby0303zjn@buaa.edu.cn, wangyu@buaa.edu.cn).

C. Cheng is with the Department of Mathematics and Computer Science, Colorado College, CO 80946, United States (e-mail: d_cheng@coloradocollege.edu).

*Corresponding author, e-mail: wangyu@buaa.edu.cn.

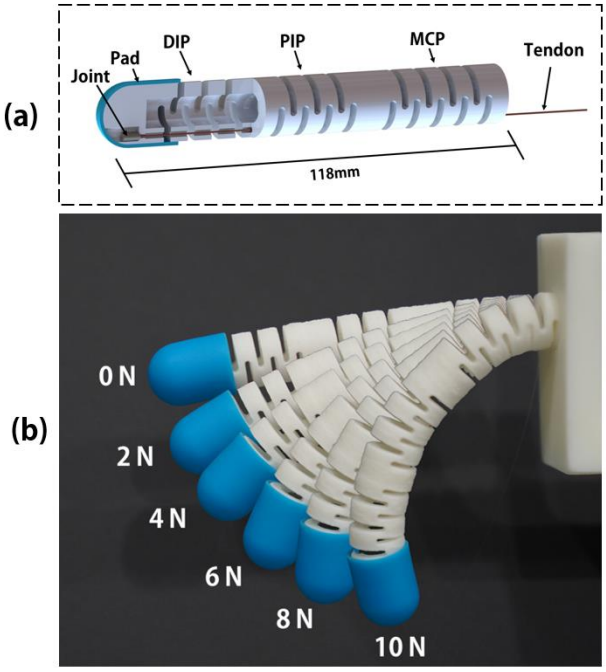

Fig. 2 The bionic finger. (a) The finger structure. (b) Bending motion of the finger under different actuated forces.

II. The Soft Hand

A. Inspiration

The proprioception of our system inspired by the human body is shown in Fig. 1. For humans, proprioception refers to the sense of body position and load achieved primarily through joint, muscle, and tendon proprioceptors [20]. Muscle proprioceptors mainly contain muscle spindles, which are enveloping structures with spiraling afferents that deliver signals to the central nervous system. The muscle spindle is capable of encoding the stretch, length, and velocity of the muscle length change. In our perception system, the function of the muscle spindle was mimicked by a linear coder within the actuator, which signals the position and velocity of the actuator.

In addition to positional feedback, in the human body, force-specific information is provided by the Golgi tendon organs (GTO), the tendon proprioceptors. Tendons are elastic structures that serve as interfaces between muscles and bones. The Golgi tendon organs are located at the junction between the muscles and tendons [20]. When the tensile load on a tendon increases, such as during resisted movements, the afferents that connect the corresponding GTO to the central nervous system will increase their firing frequency to deliver such information. In our system, a one-dimensional force sensor embedded in the tendon performs like a GTO, which we term the bionic Golgi tendon organ (BGTO).

Besides, three types of joint proprioceptors reside within different levels of human joint anatomy, and they are sensitive to different stimulus frequencies. These receptors have the property of firing when the joint reaches a certain angular threshold, which is quite similar to mechanical angular encoders. Studies have shown that information provided by joint receptors is rather ambiguous: approximately 70% of these receptors respond only to drastic movements of the joint. Joint proprioceptors have also been marked as less important contributors to kinesthesia and the awareness of movement and position than muscle spindles [21, 22]. Therefore, in our system, bionic joint receptors were not implemented.

By using a linear encoder to mimic the muscle spindle and tension sensor to mimic GTO, our system can achieve perception. We integrated it into a bionic finger and then into a soft robotic hand.

B. Design of the Bionic Finger

We adopted the finger design from our previous work [23], which is a 3D-printed hollow continuum structure. The continuum joint is constructed by a series of notches that can flex under tendon tightening and extend under tendon release. There are 3 joints of the finger similar to a human finger (Fig. 2a). The finger length is 118 mm and the diameter is 16 mm. A rubber sleeve with a thickness of 0.5 mm was attached to the distal end of the finger as a finger pad to provide more stability for grasping. The tail of the tendon was fixed with an aluminum sheet as the tendon joint. The through-hole on the finger pipe was used for tendon through. A 0.5 mm diameter stainless steel wire was used as the tendon. The entire finger was 3D-printed using nylon material. The curved finger shapes under different tension values are shown in Fig. 2b.

C. Design of the soft hand

Based on the soft bionic finger, a three-fingered soft hand was developed (Fig. 3a). Three fingers were mounted evenly on a palm. Three force sensors (1789, Arizon) with a range of 0-20 N and a resolution of 0.01 N were attached to the tendons and worked as BGTOs. There are three cylindrical shell warps around the sensors so they can only move vertically with the palm. Three linear motors were used as the actuators of the soft hand. The lower controller is an Arduino Uno, communicating with the actuators through serial port. The sensors communicate with the upper computer through Modbus. The entire gripper can be mount on a six-DOF (degree of freedom) robotics arm to perform grasp operations.

D. Basic grasp ability of the soft hand

The basic grasp ability of the soft hand was validated experimentally under two grasp types: top grasp and side grasp. In the top grasp, the hand grasp objects from the top, exploiting the support surface to guide the operation while in the side grasp, the soft hand grasp objects from the side as the object sides along a surface. First, a series of objects were selected for grasping and some of the grasp scenes are shown in Fig. 3b-i. The soft hand can successfully grasp fragile objects such as an egg and a bulb (Fig. 3b, Fig. 3f), and proteiform objects such as a bunch of grapes and a paper cup (Fig. 3c, Fig. 3d) under simple position control. Objects with different shapes and sizes (a marker, an apple and a tennis ball) can be grasped by uniform grasp motion, which indicates adequate compliance (Fig. 3e, Fig. 3g and Fig. 3h). In Fig. 3b-h, objects were grasped by the top grasp. We also show a side grasp of the coke bottle in Fig. 3i.

The grasp forces under the top grasp and side grasp were tested. A tennis ball was used for the top grasp: the tennis ball was fixed to a digital force meter, grasped under varied actuated tendon lengths and moved the soft hand vertically until the soft hand was separated from the ball. The maximal

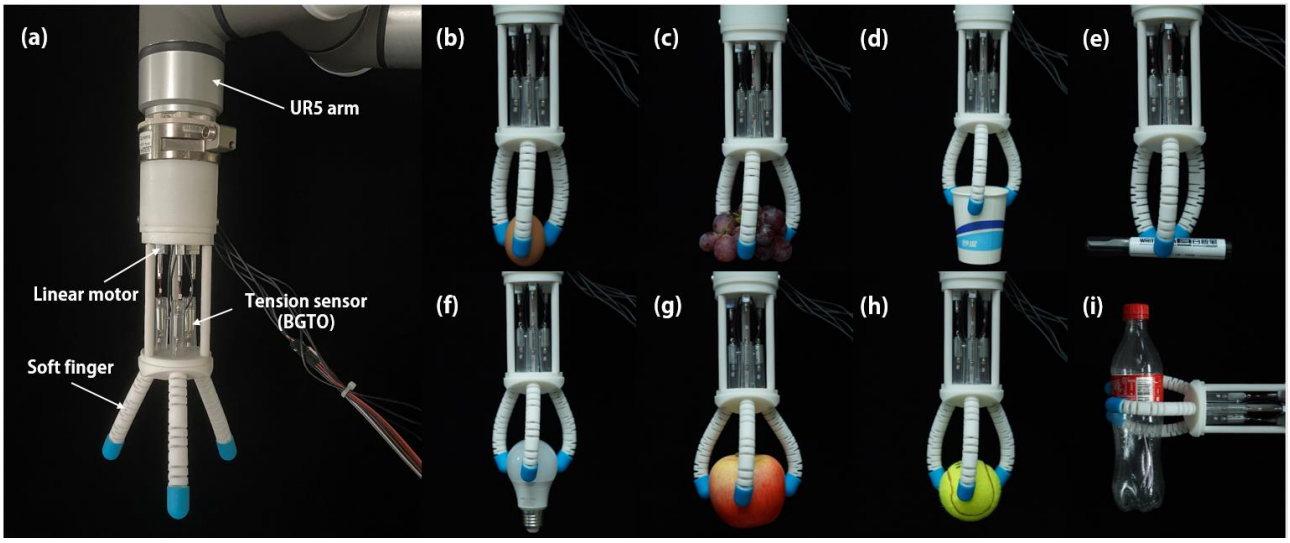

Fig. 3 The soft robotic hand. (a) The soft hand mounted on a UR5 robotic arm. (b-h) The soft hand grasped an egg, a bunch of grapes, a paper cup, a marker, a bulb, an apple and a tennis ball using the top grasp. (i) The soft hand grasped a coke bottle using the side grasp.

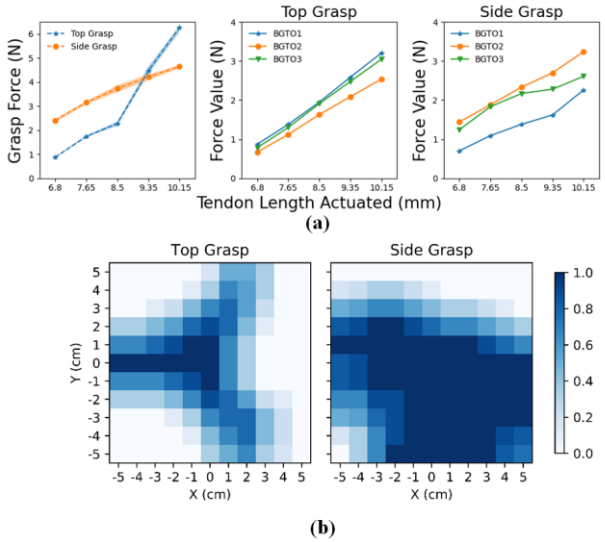

Fig. 4 Grasp force and grasp area. (a) left: the top grasp force of a tennis ball and the side grasp force of a coke bottle; middle: the force values of BGTOs of top grasp; right: the force values of the BGTOs of side grasp. (b) The grasp success rates of top grasp and side grasp under objects position uncertain.

force in this process of the force meter was recorded for each trial. Three trials were executed for each actuated tendon length and the results were averaged. During this process, the force values of the three BGTOs were recorded when the grasp motion was complete, but the hand did not move. For side grasp, a coke bottle was used, and the same method was used except that the soft hand grasped the bottle from the side and moved horizontally until separated with it. The results of this experiment are shown in Fig. 4a. We can see that a more actuated tendon length leads to a higher grasp force and tendon forces.

We evaluated the grasp ability under object positions uncertainly using the methods presented in [24, 25]. Uniformly, the top grasp and side grasp were adopted, and the objects were the same as those in the grasp force test. An 11 $\times$11 cm grid was used to offer the placed positions of the objects. For each position, the soft hand executed a programmed grasp, and the result was recorded as success or failure. In the top grasp test, the robotic hand grasped the tennis ball from the top and lifted it to a certain height after the grasp was completed. In the side grasp test, the soft hand grasped the coke bottle from the side and lifted it. A successful grasp means that the object is lifted, and there is no slip with the manipulator. To keep the number of trials to a reachable range, only a trial was conducted for each position, so for each grasp type, a total of 121 trials were recorded. A 3$\times$3 sliding window was used to filter the results by averaging the covered area. The results are shown in Fig. 4b, and it can be seen that the hand can grasp the tested object in a contiguous range of positions.

Despite the reliable grasping capacity of the proposed hand, it is worth noting that the grasping ability is not the key point of this paper. We will show the sensory ability of the soft hand in the next two sections including texture identification and object recognition.

III. Textures Identification

In this section, we evaluate the texture identification capacity of the soft bionic finger. Even if many previous works have achieved high classification accuracy of textures, it has a known limitation of requiring precise contacts, so the experimental conditions are generally constrained, such as a given actuating state or contact area between object and finger. In this paper, we set fewer constraints on the contact conditions. Texture signals were collected under random actuator displacements and five finger rotation angles. The results showed the robust texture classification ability of the finger.

A. Experiment Setup

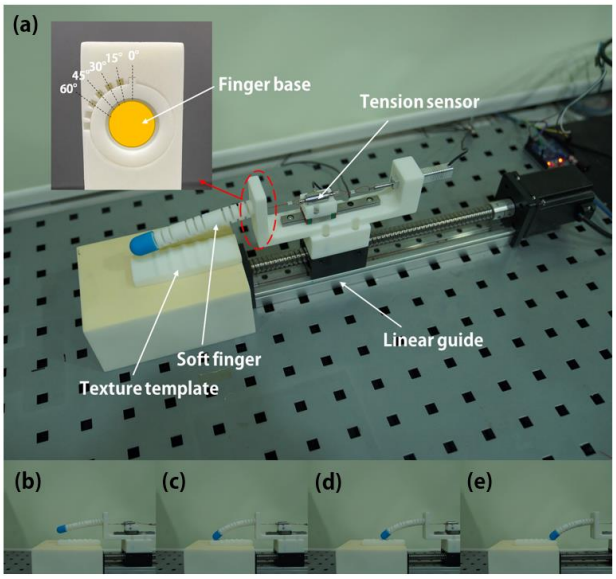

Fig. 5 (a) The experiment setup of texture classification. (b-e) Experimental Procedure.

The setup in this experiment is shown in Fig. 5a, and primarily includes a finger module, an active linear guide, and a texture template. The finger module consists of a soft bionic finger, a tension sensor working as a BGTO, a linear motor, and a support part. The soft finger was mounted on an inner base with a rectangular locating pin. The finger can be rotated to different angles depending on the mounting angle of the locating pin. In this experiment, five angles were selected: 0, 15, 30, 45 and 60 degrees. At the beginning of each trial, the linear guide carried the finger module to a certain position (Fig. 5b). Then the finger was actuated to bend to touch the front end of the texture template (Fig. 5c). To test the generalizability of the proposed system, the actuated tendon length in this phase was set to be given randomly in a workable range of 6.5-10.2 mm. "Workable" means that the finger is in contact with the template. The accuracy of the displacement of the actuator was determined by the linear encoder in this phase. After this, the finger palpated the texture template by the linear guide, which moved backward at a speed of 0.15 m/s (Fig. 5d). A trial was complete until the fingertip arrived at the tail end of the texture template (Fig. 5e). The change in tendon strain was simultaneously recorded by the BGTO at a frequency of 60 Hz. For each finger rotation angle, 20 trials were conducted, and a total of 120 trials were executed at this stage.

B. *textures design*

All texture templates were rectangular blocks with sizes of 100×30×10 mm (Fig. 6). They were 3D printed with photosensitive resin. A total of 17 textures were adopted which can be divided into five groups according to the texture shape: flat surface (F), circular grooves (C1-C4), rectangular grooves (R1-R4), triangular grooves (T1-T4) and sloped grooves (S1-S4). The textured surface was a 60 × 30 mm rectangle centered along the template.

C. *Features Extraction*

Before extracting texture features, some preprocessing is needed. The beginning and end of each trial were cropped out as they represented uniformly flat sections. Then, 200 continuous samples in the middle of the sliding process were used for the next step. Subsequently, zero-mean normalization was performed on the cropped data to compensate for the initial contact strain on the tendon. The resulting data indicate the normalized fluctuation of the tendon stress when the finger palpates different plates. To increase the randomness of the samples, a window with a length of 90 was used to further crop the continuous samples randomly. For each trial, 50 times crops were applied, so in this stage, a total of 17000 cropped samples were obtained for identification. We then extract the Fourier components of the post-preprocessing data using a fast Fourier transform (FFT). The magnitude of the Fourier components between frequencies of 0 and 30 Hz, with an interval of 0.33 Hz are used as candidate features for classification. The normalized strain data and extracted Fourier components of eight different textures are displayed in Fig. 7. The corresponding textures are R1, F, T1, S1, C1, C2, C3 and C4 from left to right successively.

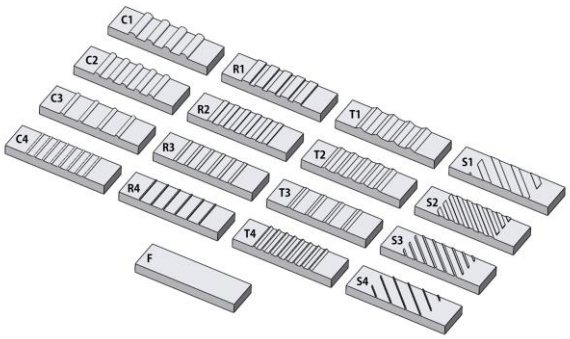

Fig. 6 The 17 texture templates

After data preprocessing, a feature selection (FS) method was used to select the most useful features. In general, an adequate FS method is vital for classification tasks, as it can decrease the dimension of the feature space and eliminate noise. In this task, we used the chi-squared to obtain a subset of the features. This method computes chi-squared stats between each non-negative feature and class. The features are then ranked according to the correlation coefficient. The number of highest-ranking n features for identification in this study was set to eight, which is a tradeoff between accuracy and efficiency.

D. *Classification algorithms*

Four classifiers were used to identify the 17 textures: support vector machines with a linear kernel (SVM-linear), support vector machines with a radial basis function kernel (SVM-rbf), K nearest neighbor (KNN) and decision trees (DTs). For KNN, the five nearest neighbors were found to output the identity of the texture. These classifiers all run in *make_pipeline* of *scikit-learn*. To validate the classification results systematically, we utilized k-fold cross validation. This method first pseudo randomly partitions the dataset into k subsets, or folds. Let there be folds of $f1$, $f2$, …, fk. As the validation begins, the learning model first omits $f1$ and trains on $f2$ to fk; it then validates on the $f1$ set and receive an accuracy. Afterward, the learning model resets and takes out $f2$ as the validation set, trains, and then validates again. This process is repeated for each of the folds, and the final accuracy

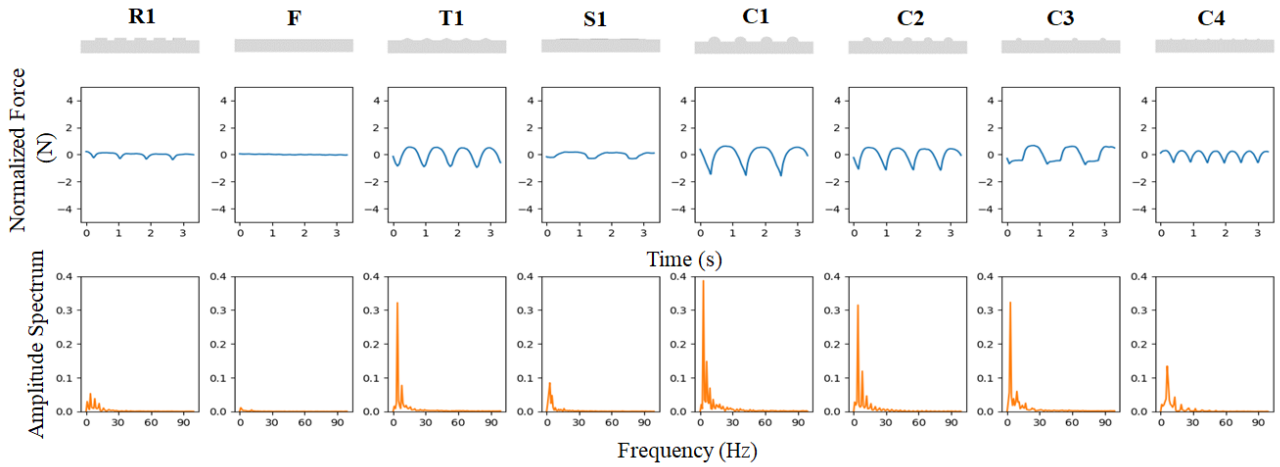

Fig. 7 Time-domain features and frequency-domain features of eight different textures.

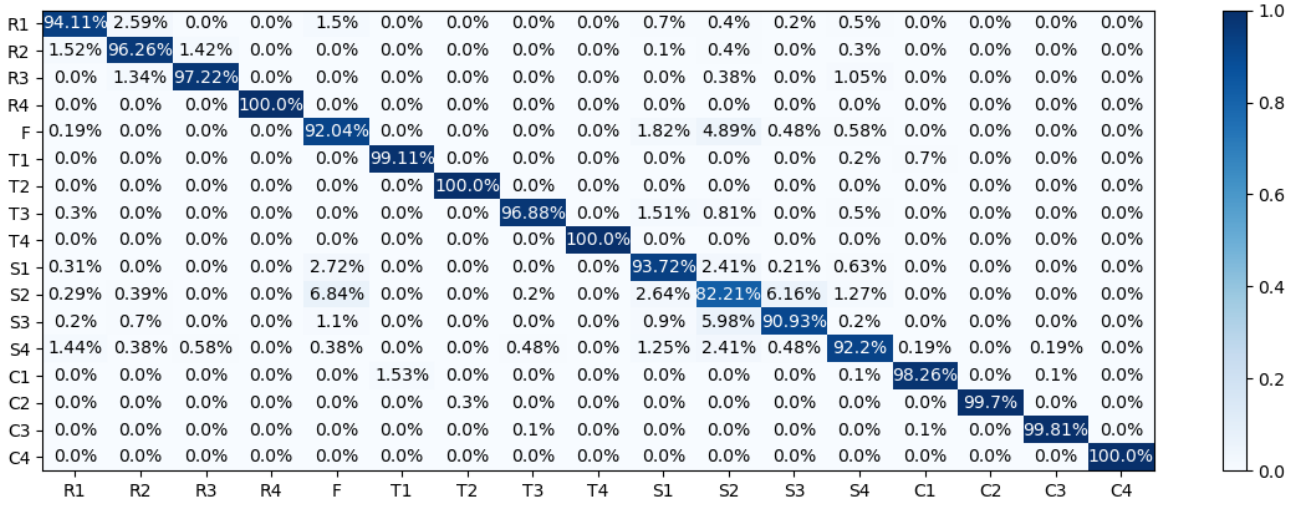

Fig. 8 Confusion matrix of DS5 using KNN classifier.

is calculated by averaging the accuracy at each fold. K-fold cross validation is often used to avoid bias or intentional training and validation set selection for embellishing machine learning performance. In our experiment, k is set at ten. We ran the 10-fold cross validation and averaged the results to obtain an overall accuracy.

To evaluate the influence of the finger rotation angle on the classification accuracy, we used five combination forms to construct the data set (DS). Five DSs were obtained: DS1 only contains the sample collected at 0 degrees of the finger rotation angle. DS2 contains the samples of 0 and 15 degrees. DS3 contains 0, 15 and 30 degrees. DS4 contains 0, 15, 30 and 45 degrees. DS5 contains all samples. Then, the textures of all five DSs were classified using the four classifiers.

E. Classification Performance

The overall identification results are listed in Table I. We can see that the KNN classifier has the best performance in this task. The average accuracy using the KNN of five DSs was 98.3%, and more than 99% accuracy was obtained for both DS1 and DS2. The confusion matrix using KNN to identify DS5 is shown in Fig. 8. The worst performing classifier was SVM-linear, with an average accuracy of

TABLE I. Overall classification accuracies for five DTs using four classifiers

Data Set	Classifier			
	SVM-linear	***SVM-RBF***	***KNN***	***DTs***
DS1	43.73%	98.97%	99.85%	98.21%
DS2	63.79%	98.21%	99.81%	98.19%
DS3	60.53%	91.38%	97.89%	94.61%
DS4	65.36%	90.63%	97.97%	94.93%
DS5	64.50%	84.28%	96.02%	91.92%

59.58%. In addition, the accuracies decreased slightly as the number of finger rotation angles involved in the DS increased. For SVM-rbf, KNN and DTs, the accuracies of DS5 were decreased by 14.69%, 3.83% and 6.29% compared with DS1, indicating that the randomness of finger rotation angles did affect the results. For the SVM-linear classifier, the irregular change in accuracy implied that the textures are hard to linearly identify in a low-dimensional feature space.

Overall, the high accuracies using SVM-rbf, KNN and DTs indicate the high-performance texture discrimination ability

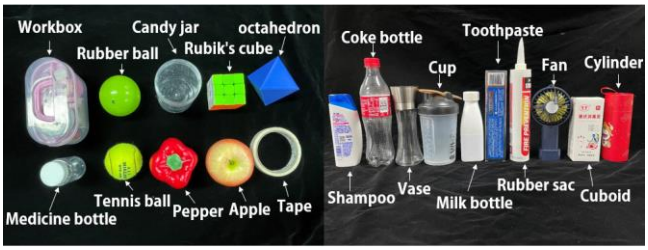

Fig. 9 Objects for recognition.

of the proposed bionic finger. Considering the random contact force and finger rotation angle variation, the results imply high robustness and possibility for application in realistic environments.

IV. Objects Recognition

In this section, we used two approaches to recognize different objects. For objects with distinct shapes, the static forces of three BGTOs were used for recognition, while the dynamic changes of three BGTOs were used to recognize objects with similar shapes.

A. Objects varied in shape

Soft manipulators can complete grasp manipulation without sophisticated control, owing to inherent compliance. Even under a uniform actuated state, the finger configuration varies according to the shape and stiffness of the object. Accordingly, for tendon-driven manipulators, the tendon tensions are distinct when grasping under this condition. Given this characteristic, we can classify objects with tendon tensions, which implies the shape information of the objects. In this study, for a single grasp, a three-dimensional force space was defined with the force values of three BGTOs. Objects can be classified according to their position in this space.

A total of 20 objects were selected for recognition: 10 for the top grasp and 10 for the side grasp (Fig. 9). The objects selected for top grasp are a workbox, a medicine bottle, a rubber ball, a tennis ball, a candy jar, a pepper, a Rubik's cube, an apple, an octahedron and a tape. The objects for side grasp are a shampoo, a coke bottle, a vase, a cup, a milk bottle, a toothpaste, a rubber sac, a fan, a cuboid and a cylinder. All the objects in this experiment were successfully grasped by our soft hand in the basic grasp ability test described in Section II. We apply a uniform actuated state to execute the grasp for all objects. For the top grasp, the object was placed in the central area with a 100% grasp success rate in Fig. 4b, at the beginning of each trial. Then, the soft hand grasped the object from the top and lifted it to a height of approximately 20 cm. The static force values of the three BGTOs when the grasp was completed were recorded as the configuration state. For each object, 20 trials were executed. For the side grasp, the procedure is nearly identical except for the soft hand grasped object from the side. In Fig. 10, we plot the three-finger tension distribution of each object in a three-dimensional space. We can see that the positions varied roughly between different objects, which implies the hand configuration.

The four classifiers in Section III were used to identify the objects, and the distance was calculated via the Euclidean metric on the three-dimensional force point. A 10-fold cross

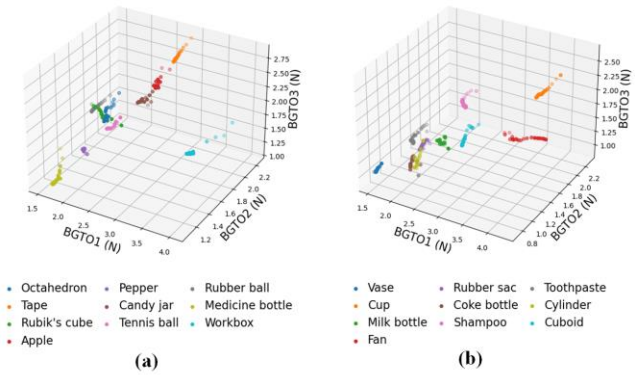

Fig. 10 The distribution of objects in a three-dimensional force space. (a) Top grasp. (b) Side grasp.

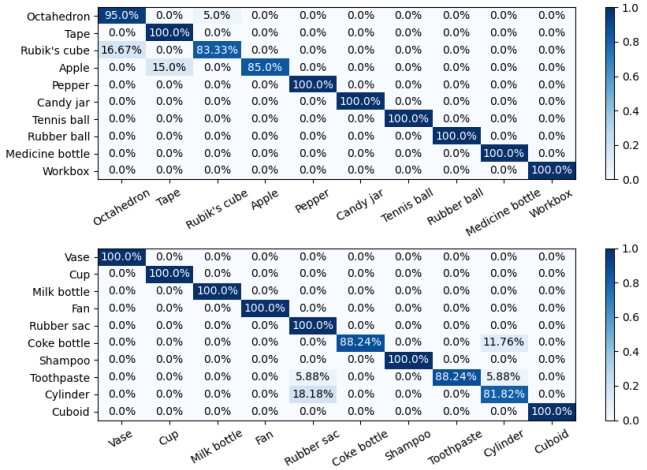

Fig. 11 The confusion matrixes of objects recognition using KNN classifier (upper: top grasp; lower: side grasp).

TABLE II. Overall Classification Accuracies of Objects Recognition Using Four Different Classifiers

Grasp type	Classifier			
	SVM-linear	***SVM-RBF***	***KNN***	***DTs***
Top grasp	84.21%	88.06%	96.33%	93.50%
Side grasp	79.1%	80.47%	95.82%	96.00%

validation was performed to obtain averaged accuracies. The results are listed in Table II. We can see that the highest accuracy of the top grasp was 96.33% by KNN and that of the side grasp was 96.00% by DTs. Neither SVM-linear nor SVM-rbf performed well in this task with accuracies of less than 90%. The recognition confusion matrixes under the top grasp and side grasp using KNN are shown in Fig. 11. For the top grasp, misclassification mainly occurs between the octahedron and Rubik's cube. There is a probability of 16.67% Rubik's cube misclassified as an octahedron and the inverse is 5.0%. Apple has a rate of 15.0% misclassified as Tape. For the side grasp, the coke bottle has a probability of 11.76% being misclassified as a cylinder, toothpaste has a rate of 5.88% being misclassified as a rubber sac and cylinder, respectively, and the cylinder has a rate of 18.18% being misclassified as a rubber sac. For these failed identification cases, we can see from Fig. 10 that the confused objects are close in the three-dimensional space, which indicates a similar grasp configuration of the hand.

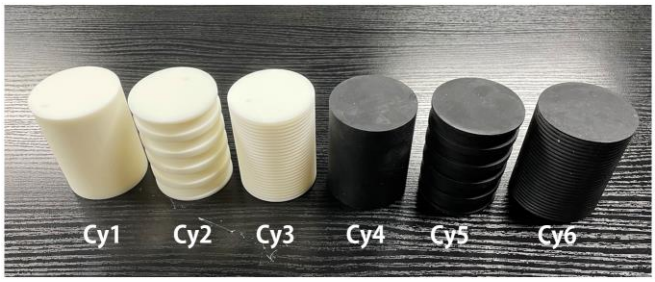

Fig. 12 Six cylinders with same outer dimensions for recognition.

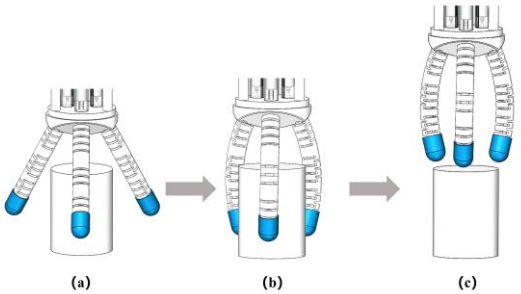

Fig. 13 The process of scan-grasp.

B. *Objects with similar dimension*

The results in the subsection above show that the capacity to identify objects varies in shape. However, it is difficult to distinguish objects with similar geometries using the proposed mechanism. In this case, the hand configuration when the grasp was completed was close, leading to confusion. In this subsection, a novel approach named "scan-grasp" was presented to distinguish objects with the same shape.

Six 3D-printed cylinders (Cy1-Cy6) with the same out dimensions (height: 80 mm, diameter 60 mm) were used for classification (Fig. 12). Cy1-Cy3 were 3D-printed by polylactic acid (PLA), which are comparatively hard. Cy4-Cy6 were hollow and made with silicone, so they were soft compared with Cy1-Cy3. Cy1 and Cy4 have a smooth surface, Cy2 and Cy5 have the same square bulges on their surface, and Cy3 and Cy6 have the same semicircular bulges on their surface.

We used a "scan-grasp" approach to grasp these cylinders (Fig. 13): first fix the cylinder and move the hand to the top of it (Fig. 13a). Then, grasp it used a "workable" actuated state (Fig. 13b). In this step, the actuated tendon lengths of the three fingers were identical, and randomly assigned. "Workable" means the fingers and cylinder were actually in contact after grasping was completed. Finally, the hand was moved vertically to "scan" the cylinder until the hand separated from the cylinder (Fig. 13c). The force values of the three BGTOs were recorded throughout the entire process. For each cylinder, 20 trials were executed. A data processing method similar to that described in Section III was used to acquire the candidate frequency features of each finger. The final eight features were selected using the chi-square method from the candidate features of all three fingers. The raw force values and frequency amplitudes of the six scan-grasp are shown in Fig. 14. Then, the three high-performance classifiers in Section III, namely, SVM-rbf, KNN and DTs, were used to identify the six cylinders.

TABLE III. OVERALL ACCURACIES FOR THREE TYPES OF THREE CLASSIFIERS

Characteristics of classification	Classifier		
	SVM-RBF	***KNN***	***DTs***
Stiffness	99.23%	98.46%	99.23%
Surface texture	65.38%	96.15%	95.38%
Integrated stiffness and texture	80.77%	97.69%	96.92%

There were three purposes in this experiment: identifying hard cylinders (Cy1-Cy3) and soft cylinders (Cy4-Cy6); identifying smooth cylinders (Cy1, Cy4), square-bulge cylinders (Cy2, Cy5) and semicircular cylinders (Cy3, Cy6); and identifying all six cylinders. Therefore, the labels of each cylinder were assigned according to the three identification purposes. The results are listed in Table III. We can see that when the cylinders were labeled soft and hard, the classifiers had the best performance, and the accuracies of SVM-rbf, KNN and DTs were all greater than 98%. For the other two types of identification, the accuracies of KNN and DTs were all greater than 95%, but SVM-rbf did not perform well, with accuracies of 65.38% and 80.77%. As a whole, our soft hand could recognize the six cylinders according to their stiffness, textures, or the combinations.

V. CONCLUSION AND FUTURE WORK

In this paper, we present a bionic approach to achieve reliable perception of a robotic hand. By mimicking the proprioception of the human body into a soft finger, 17 textures were accurately classified under distinct finger rotation angles and actuator displacements with the highest average accuracy of 98.3%. The design of the bionic framework was detailed. Based on this, a three-fingered soft hand was constructed. Its basic grasp ability was evaluated with two types of grasps. The object recognition capacity was experimentally verified. For objects that varied in shape and had similar dimensions, two different approaches were adopted to recognize them. The average recognition accuracies were 95.5% and 98%, respectively.

The proposed sensory system is robust and has fine environmental adaptability. This approach can be easily applied to other tendon-drive systems. In addition, bionic design makes it convenient to apply to prosthetic hands because the signal can be easily converted into neuromorphic spike trains. In some previous work, researchers have brought sensing to amputees using neuromorphic methods [26]. However, there are still some problems in this study. For instance, the textures identified in this paper are rough on a visual scale. Furthermore, we can explore the recognition ability of fine textures. The characteristics of the sensor are also critical for perception. A better resolution and response speed may improve the results. In the feature selection part, other methods can be used to select candidate features, such

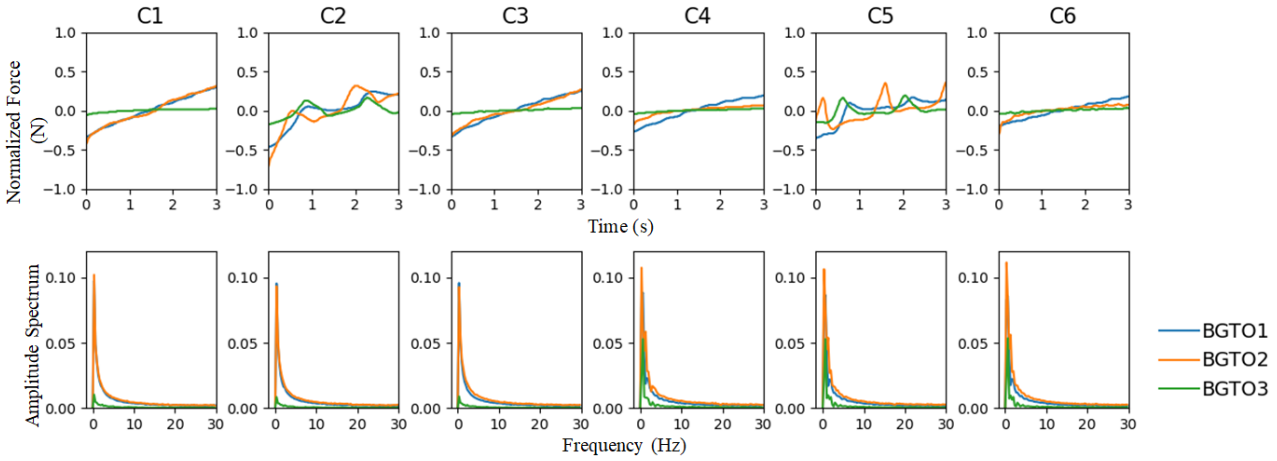

Fig. 14 Time-domain features and frequency-domain features of six cylinders.

as some widely used features in EMG signal processing. In addition, for object recognition, the algorithm is sensitive to the poses of the objects placed. Excessive pose changes may affect the recognition accuracy. In the future, more complex algorithms can be used to solve this problem. We also noticed that increasing the number of tendons of a single finger and BGTOs can bring more perceptual possibilities. In the future, we will further investigate the sensory ability of the bionic approach.

REFERENCES

[1] Deimel, Raphael, Brock, and O. J. I. J. o. R. Research, "A novel type of compliant and underactuated robotic hand for dexterous grasping," 2016.

[2] Y. Hao, S. Biswas, E. W. Hawkes, T. Wang, and Y. J. I. T. o. R. Visell, "A Multimodal, Enveloping Soft Gripper: Shape Conformation, Bioinspired Adhesion, and Expansion-Driven Suction," vol. PP, no. 99, pp. 1-13, 2020.

[3] D. L. Rus and M. T. J. N. Tolley, "Design, fabrication and control of soft robots," vol. 521, no. 7553, pp. 467-475, 2015.

[4] S. Abondance, C. B. Teeple, R. J. J. I. R. Wood, and A. Letters, "A Dexterous Soft Robotic Hand for Delicate In-Hand Manipulation," vol. PP, no. 99, pp. 1-1, 2020.

[5] J. Zhou *et al.*, "A Soft-Robotic Approach to Anthropomorphic Robotic Hand Dexterity," vol. 7, pp. 1-1, 2019.

[6] Z. Jianshu, Y. Juan, C. Xiaojiao, L. Zixie, W. J. I. R. Zheng, and A. Letters, "BCL-13: A 13-DOF Soft Robotic Hand for Dexterous Grasping and In-Hand Manipulation," vol. PP, pp. 1-1, 2018.

[7] R. S. Dahiya, G. Metta, M. Valle, and G. J. I. T. o. R. Sandini, "Tactile Sensing—From Humans to Humanoids," vol. 26, no. 1, pp. 1-20, 2010.

[8] R. S. Dahiya, P. Mittendorfer, M. Valle, and G. J. I. S. J. Cheng, "Directions Toward Effective Utilization of Tactile Skin: A Review," vol. 13, no. 11, pp. 4121-4138, 2013.

[9] M. Rasouli, C. Yi, A. Basu, S. L. Kukreja, N. V. J. I. T. o. B. C. Thakor, and Systems, "An Extreme Learning Machine-Based Neuromorphic Tactile Sensing System for Texture Recognition," vol. 12, no. 99, pp. 313-325, 2018.

[10] Y. Cao, T. Li, G. Yang, L. Hui, and T. J. S. Zhang, "Fingerprint-Inspired Flexible Tactile Sensor for Accurately Discerning Surface Texture," vol. 14, no. 16, p. 1703902, 2018.

[11] N. Jamali and C. J. I. T. o. R. Sammut, "Majority Voting: Material Classification by Tactile Sensing Using Surface Texture," vol. 27, no. 3, pp. 508-521, 2011.

[12] N. Jamali, C. J. P. I. I. C. o. R. Sammut, and Automation, "Slip prediction using Hidden Markov models: Multidimensional sensor data to symbolic temporal pattern learning," 2012.

[13] S. Sankar, D. Balamurugan, A. Brown, K. Ding, and N. Thakor, "Texture Discrimination with a Soft Biomimetic Finger Using a Flexible Neuromorphic Tactile Sensor Array That Provides Sensory Feedback," 2020.

[14] M. Amjadi, K. U. Kyung, I. Park, and M. J. A. F. M. Sitti, "Stretchable, Skin-Mountable, and Wearable Strain Sensors and Their Potential Applications: A Review," vol. 26, no. 11, 2016.

[15] H. Zhao, K. O'Brien, S. Li, and R. F. J. S. R. Shepherd, "Optoelectronically innervated soft prosthetic hand via stretchable optical waveguides," vol. 1, no. 1, p. eaai7529, 2016.

[16] C. To, T. L. Hellebrekers, and Y. L. Park, "Highly stretchable optical sensors for pressure, strain, and curvature measurement," in *IEEE/RSJ International Conference on Intelligent Robots & Systems*, 2015.

[17] B. S. Homberg, R. K. Katzschmann, M. R. Dogar, and D. J. A. R. Rus, "Robust proprioceptive grasping with a soft robot hand," 2018.

[18] L. Scimeca, J. Hughes, P. Maiolino, F. J. I. R. Iida, and A. Letters, "Model-free Soft-Structure Reconstruction for Proprioception using Tactile Arrays," pp. 1-1, 2019.

[19] G. Li, S. Liu, L. Wang, and R. J. S. R. Zhu, "Skin-inspired quadruple tactile sensors integrated on a robot hand enable object recognition," vol. 5, no. 49, p. eabc8134, 2020.

[20] J. C. Tuthill and E. J. C. B. C. Azim, "Proprioception," vol. 28, no. 5, p. R194, 2018.

[21] P. Grigg, G. A. Finerman, and L. H. J. J. Riley, "Joint-position sense after total hip replacement," vol. 55, 1973.

[22] F. J. Clark, K. W. Horch, S. M. Bach, and G. F. J. J. o. N. Larson, "Contributions of cutaneous and joint receptors to static knee-position sense in man," vol. 42, no. 3, pp. 877-888, 1979.

[23] Y. Yan, Y. Wang, X. Chen, C. Shi, J. Y. and, and C. Cheng, "A tendon-driven prosthetic hand using continuum structure*," presented at the 2020 42nd Annual International Conference of the IEEE Engineering in Medicine & Biology Society (EMBC), 2020.

[24] R. Deimel and O. Brock, "A compliant hand based on a novel pneumatic actuator," in *IEEE International Conference on Robotics & Automation*, 2013.

[25] M. Kazemi, J. S. Valois, J. A. Bagnell, and N. Pollard, "Robust Object Grasping using Force Compliant Motion Primitives," in *Robotics: Science and Systems 2012*, 2012.

[26] S. Sankar, A. Brown, D. Balamurugan, H. Nguyen, and N. Thakor, "Texture Discrimination using a Flexible Tactile Sensor Array on a Soft Biomimetic Finger," in *2019 IEEE SENSORS*, 2019.